

# Molecular Dynamics of Folding of Secondary Structures in Go-Like Models of Proteins

Trinh Xuan Hoang and Marek Cieplak  
*Institute of Physics, Polish Academy of Sciences, Warsaw, Poland*

Correspondence to:

Marek Cieplak  
 Institute of Physics,  
 Polish Academy of Sciences,  
 Aleja Lotników 32/46,  
 02-668 Warsaw, Poland  
 Tel: (48-22) 843-66-01 ext. 3365  
 Fax: (48-22) 843-09-26  
 E-mail: mc@maja.ifpan.edu.pl

## Abstract

We consider six different secondary structures of proteins and construct two types of Go-like off-lattice models: with the steric constraints and without. The basic aminoacid-aminoacid potential is Lennard Jones for the native contacts and a soft repulsion for the non-native contacts. The interactions are chosen to make the target secondary structure be the native state of the system. We provide a thorough equilibrium and kinetic characterization of the sequences through the molecular dynamics simulations with the Langevin noise. Models with the steric constraints are found to be better folders and to be more stable, especially in the case of the  $\beta$ -structures. Phononic spectra for vibrations around the native states have low frequency gaps that correlate with the thermodynamic stability. Folding of the secondary structures proceeds through a well defined sequence of events. For instance,  $\alpha$ -helices fold from the ends first. The closer to the native state, the faster establishment of the contacts. Increasing the system size deteriorates the folding characteristics. We study the folding times as a function of viscous friction and find a regime of moderate friction with the linear dependence. We also consider folding when one end of a structure is pinned which imitates instantaneous conditions when a protein is being synthesized. We find that, under such circumstances, folding of helices is faster and of the  $\beta$ -sequences slower.

**Keywords:** protein folding; Go model; molecular dynamics; secondary structures

Understanding of the statistical mechanics aspects of protein folding has been recently advanced through studies of coarse grained models in which aminoacids are represented by single beads. In particular, many valuable insights have been gained by considering such models on a lattice (see, e.g. Chan & Dill, 1993; Dill et al., 1995; Cieplak et al., 1998). These toy models have allowed one to relate the folding process to the sequence dependent energy landscapes (Chan & Dill, 1994; Wolynes, 1996; Sali et al., 1994), to identify the folding pathways (Chan & Dill, 1998), and to study the issues of designability (Li et al., 1996; Vendruscolo et al., 1997). They have also been used to demonstrate existence of tree like kinetic connectivities in the folding funnel (Garstecki et al., 1999; see also Miller & Wales, 1999) that can be represented with the use of the disconnectivity graphs (Becker & Karplus, 1997).

More realistic coarse grained models, however, require an off-lattice setting. Recently, there have been a number of off-lattice studies, which focus on the kinetics of folding (Iori et al., 1991; Irback et al., 1997; Veithshans et al., 1997; Dokholyan et al., 1998; He & Scheraga, 1998; Hardin et al., 1999), as well as on the sequence design and determination of the interaction potentials (Kolinski et al., 1995; Irback et al., 1997; Clementi et al., 1998). It has been also suggested that the geometry of the native structure of proteins itself, without a detailed information regarding the amino acid sequences, plays a decisive role in the folding process (Micheletti et al., 1999). The effective interactions between the beads in the coarse-grained models are difficult to derive from microscopic considerations and instead they may be chosen to reflect statistical properties of protein structures as collected in the Protein Data Bank (Miyazawa & Jernigan, 1985; Kolinski et al., 1995).

The advantage of the lattice models is that they allow for an enumeration of conformations, at least for short chains, and thus for identification of the native state and determination of equilibrium properties of the system. However, the dynamics of these models are not related to any Newton's equations (in the classical limit) since they have to be defined in terms of the discrete Monte Carlo steps made within a declared set of allowed moves.

Molecular dynamics (MD) simulations are a natural tool to study models set in a continuum space independent of whether they are coarse-grained or fully atomic. A decade ago, MD simulations of the microscopic representation of a polypeptide chain could explore time scales which were around nanoseconds and thus orders of magnitude too short to study the full duration of a typical folding (Karplus, 1987). Currently, microsecond time

scales have become accessible (Duan & Kollman, 1998) (in a special purpose computer) but these feats allow one to monitor individual trajectories in very restricted regions of the phase space. A detailed characterization is still restricted to up to  $10\text{ns}$  long time scales (Boczek & Brooks, 1995). Thus such chemically realistic models cannot yet provide a sufficiently thorough equilibrium and kinetic characterizations of the system that are expected when setting up a model to be studied within the framework of statistical mechanics.

Thus there is a need to study simplified coarse-grained continuum space models to understand the generic features of folding. These models must involve idealized potentials, for instance of the Lennard-Jones kind. These interactions may either be constrained to correspond to a target native state or not (Iori et al., 1991). The targeting may be facilitated by augmenting the model by an introduction of steric constraints (Veithshans et al., 1997; He & Scheraga, 1998), which takes into account the properties of the peptide bonds, but it can also be accomplished without such constraints (Li & Cieplak, 1999). The dynamics of the simplified Lennard-Jones models are usually studied by the methods of MD. A novel and efficient variant of the MD technique has been recently proposed by He & Scheraga (1998) in which one focuses the evolution on the torsional degrees of freedom. Some Monte Carlo studies for those models are also available (Iori et al., 1991; Irback et al., 1997; Li & Cieplak, 1999). The applicability of the Monte Carlo methods to dynamical properties (as opposed to equilibrium) remains, however, untested.

In this paper, we report on molecular dynamics studies of possibly the simplest models with the native states defined by target conformations – the off-lattice versions of the Go models (Go & Abe, 1981). The interesting property of the Go model is that it essentially avoids the issue of the correct specification of the aminoacid-aminoacid interaction and yet it corresponds to a realistic conformation by defining the couplings in terms of the target conformation. Specifically, we consider the Lennard-Jones interactions between the beads and make them attractive for native contacts (two non-contiguous beads form a contact if they do not exceed a certain cut-off distance) and repulsive for non-native contacts. Such models are protein-like also in the sense that they minimize the structural frustration. The object of our studies here is to investigate how viable are such Lennard-Jones-Go models in the context of the kinetics of protein folding. Our motivation for performing these studies follows from the expectation that such models may play a role similar to that of the Ising spin models in representing properties of the more complicated real life magnetic systems.

Recently, there have been several related studies of the coarse-grained off-lattice Go models which, however, asked different questions than in this paper and were not based on the Lennard-Jones potentials. The study by Zhou and Karplus (1999), employed a square well po-

tential (also used before to analyze homopolymers by Zhou et al., 1996) which leads to a simplified discrete MD treatment. The authors have studied possible scenarios (with or without long-lasting intermediates) of the folding kinetics in a three-helix-bundle-like protein model as a function of the strength of the non-native contacts relative to the strength of the native ones. This kind of discrete MD have been also used by Dokholyan, Buldyrev, Stanley and Shakhnovich (1998) to identify a folding nucleus in a Go-like heteropolymer. (For a related full atom study of this issue for the CI2 protein see Li & Daggett, 1994). Another study, by Hardin, Luthey-Schulzen, and Wolynes (1999) used a detailed backbone representation and implemented an associative memory Hamiltonian in which the contact potentials are set to be the Gaussian functions. This study was aimed at understanding the kinetics of the secondary structures formation from the perspective of the energy landscape picture. Our partiality to the Lennard-Jones potentials is of a twofold nature. First, these potentials are well established in simulations of liquids and – essentially – continuum time stable MD codes are available. Second, their overall distance dependence seems qualitatively correct on a fundamental level.

Real life conformations of proteins in the native state consist of interconnected secondary structures such as  $\alpha$ -helices,  $\beta$ -hairpins (see, e.g. Blanco et al., 1998), and  $\beta$ -sheets. Understanding of the kinetics of protein folding should be first accomplished at the level of the secondary structures. This is, in fact, the task of this paper and we narrow it to two classes of the Go models: with and without the steric constraints and for each of these we consider six possible secondary structures with different numbers of monomers. The kinetics of folding are studied by the standard techniques of MD with a Langevin noise which controls the temperature of the systems and, at the same time, mimics the interactions of the protein fragments with the molecules of water.

Our method of constructing the off-lattice Go models is outlined in the next section. We then determine the sizes of the native basins of the models through the shape distortion method (Li & Cieplak, 1999) instead of making assumptions about them, as it is done usually. Next, we determine the phononic spectra of the models and discuss their relationship to the thermodynamic stability of the native structures. We then determine the folding times, the thermodynamic stability and other characteristic parameters for the models without the steric constraints and find that the  $\beta$ -structures have very low thermodynamic stability in this model. The folding times vary with the native conformation and the chain length. In particular, the  $\alpha$ -helix folds faster than the  $\beta$ -hairpin of the same length. The latter also folds much slower than a similarly sized  $\beta$ -sheet with three strands. Experiments on folding indicate that the folding time for the hairpin is about 30 times slower than that for the  $\alpha$ -helix (Munoz et al., 1997). Our results do not yield the same rate but, at least, they show that the  $\beta$ -hairpin is the slower

folder. A similar result has been obtained by Hardin et al. (1999). Our studies of the three sizes of the helices confirm the general observation that folding properties deteriorate with the growth of the system size (Cieplak et al., 1999). We repeat the MD studies for the models with the steric constraints and find that these constraints substantially improve the thermodynamic stability, especially for the  $\beta$ -structures. At the same time, however, they raise the temperature of the onset of the glassy effects so the net result is that the  $\alpha$ -helices remain good folders and the  $\beta$ -structures remain non-optimal folders but their foldability is improved. Notice, however, that our models allow for good or adequate folding, depending on the system, without any additional dipole-dipole interactions as introduced by He & Scheraga (1998).

In a following section, we focus on the mechanisms of folding and discuss an average sequencing of events that takes place in folding of the secondary structures. In particular, we investigate characteristic time separations between the folding steps. In general, the time separations may depend on details of a model but the sequencing is expected to be model independent, i.e. it should proceed as predicted by our Go-like models. Next, we study the dependence of our results on the strength of viscous damping in the Langevin noise and find that it affects the folding time but it does not affect any of the other characteristic parameters except when the friction is set unrealistically low. Finally, we consider the processes of folding occurring when one end of the structure is fixed in space which imitates conditions found when a protein is being synthesized (Stryer, 1993). We find that fixing one end of a helix accelerates folding and improves overall folding characteristics. The folding is found to originate at the unclamped end. On the other hand, folding of the  $\beta$  structures becomes worse when one end is clamped.

This paper sets the stage for studies of full proteins and kinetic interplays between various secondary structures. Results of such studies for the Go models of proteins will be presented in a separate paper.

## MODELS

We represent a polypeptide in a simplified manner: by a chain of connected beads. The beads' positions correspond to the locations of the  $\text{C}\alpha$  atoms. When the system is in its native state, the beads have no kinetic energy and the locations of the  $\text{C}\alpha$  atoms can be obtained from the Protein Data Bank. However, the secondary structures that we study are idealized and are not targeted to a specific real structure. Instead, they are just meant to be constructed in a way which is very close to typical  $\alpha$ -helices and  $\beta$ -sheets found in the native states of real proteins. These secondary structures are stabilized primarily by the hydrogen bonds. The structures that we study are shown in Figure 1. These are: three  $\alpha$ -helices, denoted as H10, H16 and H24, two  $\beta$ -hairpins, denoted

as B10 and B16, and a  $\beta$ -sheet, B15. The numbers in the labels indicate the numbers of beads in the structures.

All of the bonds between two consecutive beads along the chain of the helices, i.e. the peptide bonds, are assumed to have the same length of  $d_0 = 3.8\text{\AA}$  which is a typical real life value. As one proceeds along the axis of the helix (the  $z$ -coordinate) from one bead to another, the bead's azimuthal angle is rotated by  $100^\circ$  and the azimuthal length is displaced by  $1.5\text{\AA}$  which again corresponds to a typical geometry.

Each of the  $\beta$ -hairpins, B10 and B16, has two anti-parallel strands which are connected by a turn. In the B15  $\beta$ -sheet there are three strands and two turns. In the  $\beta$ -structures, the strands are not straight lines but have a zigzagged geometry as shown in Figure 1. The bond lengths between two connected beads are equal to  $3.8\text{\AA}$  but the displacement along the strand direction (the  $z$  axis in Figure 1) is  $3.5\text{\AA}$ . The distance between two opposite beads in two bonded strands, is set to  $5\text{\AA}$ , which is roughly equal to the hydrogen bond's length. The turn region is constructed so that the bond length and the zigzag pattern match.

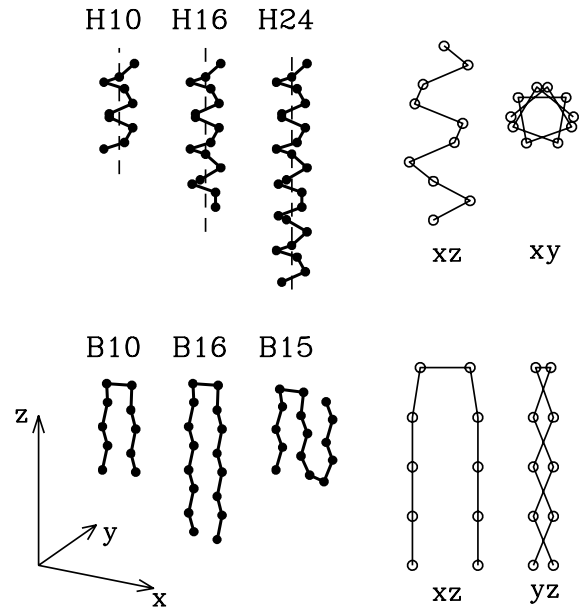


Fig. 1. Stereographic projections of the target structures studied in this paper: three  $\alpha$ -helices H10, H16, H24, two  $\beta$ -hairpins B10, B16, and a  $\beta$ -sheet B15. The  $xz$  and  $yz$  planar projections for H10 and B10 are shown on the right hand side.

The potentials of interactions between pairs of the beads are constructed in a way that ensures that the target structure coincides with the ground state of the system, i.e. with the native state. We pick the pair potentials to be of the Lennard-Jones type and select the parameters in a Go-like fashion (Go & Abe, 1981) so that significant attraction is associated with the native con-

tacts and the non-native contacts are purely repulsive. In our model, we assume that a native contact is present if the distance between the two monomers in the designed structure is shorter than  $7.5\text{\AA}$ .

These Go-like couplings already stabilize the structures under studies but that stabilization will be found here not to be sufficiently adequate, especially in the case of the hairpins. We thus consider two classes of models: with and without additional steric constraints. The steric constraints add extra stability and they take into account the directional character of the peptide bonds in a more realistic manner.

### Go-like model with no steric constraints

This model is similar in spirit to that introduced by Iori, Marinari, and Parisi (1991) and to that studied by Li and Cieplak (1999). The conceptual difference between these two papers is that the former is not constructed in reference to any predetermined target structure. For a conformation defined by the set of position vectors  $\{\mathbf{r}_i\}$ ,  $i = 1, 2 \dots N$ , the potential energy is assumed to take the following form

$$E_p(\{\mathbf{r}_i\}) = V^{BB} + V^{NAT} + V^{NON} . \quad (1)$$

The first term represents rigidity of the backbone potential, the second term corresponds to interactions in the native contacts and the third term to those in the non-native contacts.  $N$  denotes the number of residues.

The backbone potential takes the form of the sum over harmonic (Iori et al., 1991) and anharmonic (Clementi et al., 1998) interactions

$$V^{BB} = \sum_{i=1}^{N-1} [k_1(r_{i,i+1} - d_0)^2 + k_2(r_{i,i+1} - d_0)^4], \quad (2)$$

where  $r_{i,i+1} = |\mathbf{r}_i - \mathbf{r}_{i+1}|$  is the distance between two consecutive beads;  $d_0 = 3.8\text{\AA}$ ,  $k_1 = \epsilon$  and  $k_2 = 100\epsilon$ , where  $\epsilon$  is the Lennard-Jones energy parameter corresponding to a native contact.

The interaction between residues that form a native contact in the target structure is taken to be of the Lennard-Jones form:

$$V^{NAT} = \sum_{i < j}^{NAT} 4\epsilon \left[ \left( \frac{\sigma_{ij}}{r_{ij}} \right)^{12} - \left( \frac{\sigma_{ij}}{r_{ij}} \right)^6 \right], \quad (3)$$

where the sum is over all pairs of residues  $i$  and  $j$  (but those which are immediate neighbors along the chain) which form the native contacts in the given target structure.  $r_{ij} = |\mathbf{r}_i - \mathbf{r}_j|$  is the monomer to monomer distance. The parameters  $\sigma_{ij}$  are chosen in a way that each contact in the native structure is stabilized at the minimum of the potential. Essentially,  $\sigma_{ij} = 2^{-1/6} \cdot d_{ij}$ , where  $d_{ij}$  is the corresponding native contact's length.

Residues not forming the native contacts interact via a repulsive soft core potential. Our potential for non-native contacts, given below, differs from the model of Iori *et al.* in that it falls to 0 after some cut-off distance,  $d_{cut}$ . The purpose of the cutoff is to minimize structural frustration and thus to improve foldability.

$$V^{NON} = \sum_{i < j}^{NON} V_{ij}^{NON}, \quad (4)$$

$$V_{ij}^{NON} = \begin{cases} 4\epsilon \left[ \left( \frac{\sigma_0}{r_{ij}} \right)^{12} - \left( \frac{\sigma_0}{r_{ij}} \right)^6 \right] + \epsilon, & r_{ij} < d_{cut} \\ 0, & r_{ij} \geq d_{cut}. \end{cases} \quad (5)$$

Here,  $\sigma_0 = 2^{-1/6} \cdot d_{cut}$ . For distances shorter than  $d_{cut}$  the potential is purely repulsive. For the  $\alpha$ -helices we chose  $d_{cut} = \langle d_{ij} \rangle \approx 5.5\text{\AA}$  which seems to be a natural choice. For the  $\beta$ -structures, however, such a choice of  $d_{cut}$  leads to an instability of the native conformation due to a substantial energy degeneracy of the nearby conformations. A sufficient extending of the cutoff removes the degeneracy and stabilizes the native state. We have found that an adequate choice for the  $\beta$ -structures is to take  $d_{cut} = 7.5\text{\AA}$  – the distance that defines what is a contact.

Notice that in the target structures, all native contacts are optimized while the non-native contact potentials give no contribution to the energy. Thus the target structure is indeed the native state of the system. The non-native interactions contribute only when moving away from the target.

### Go-like model with the steric constraints

In this case, the potential energy of the system is given by

$$\tilde{E}_p(\{\mathbf{r}_i\}) = V^{BB} + V^{NAT} + V^{NON} + V^{BA} + V^{DA}, \quad (6)$$

where the first three terms are identical to those in equation (1), whereas the last two terms correspond to the bond angle and dihedral angle potentials respectively. The bond angle,  $\theta_i$ , is defined as the angle between two successive vectors  $\mathbf{v}_i$  and  $\mathbf{v}_{i+1}$ , where  $\mathbf{v}_i = \mathbf{r}_{i+1} - \mathbf{r}_i$ . The dihedral angle,  $\phi_i$ , is the angle between two vector products  $\mathbf{v}_{i-1} \times \mathbf{v}_i$  and  $\mathbf{v}_i \times \mathbf{v}_{i+1}$ . Following Veithshans et al. (1997), we use the following potentials for the bond and the dihedral angles

$$V^{BA} = \sum_{i=1}^{N-2} \frac{k_\theta}{2} (\theta_i - \theta_{0i})^2 \quad (7)$$

$$V^{DA} = \sum_{i=1}^{N-3} [A(1 + \cos\phi_i) + B(1 + \cos3\phi_i)] \quad (8)$$

where  $k_\theta = 20\epsilon/(rad)^2$ ,  $A = 0\epsilon$  and  $B = 0.2\epsilon$ . Our angle dependent potentials differ from those in (Veithshans et al., 1997), since in our case we take  $\theta_{0i}$  to be, in general, site-dependent and equal to the bond angles in the native targets. For the helices, however,  $\theta_{0i}$  are uniform and equal to  $1.56157 rad$  ( $89.4714 deg$ ). For the  $\beta$ -structures,  $\theta_i$ 's in the turn region are different from those in the strands.

Introduction of the steric constraints to the model described by eq. (1) shifts the native state away from the target conformation because the target need not correspond to a minimum of the dihedral potentials. However, we have found that for our choice of the parameters  $A$  and  $B$  the true native states differ only little from the targets. The true native states are found by a multiple zero temperature quench procedure from low energy conformations generated by MD trajectories that start in the target conformation. The conformation distances from the native states to the targets (to be defined in the next section) never exceeded  $0.05\text{\AA}$ .

It should be pointed out that none of the models studied here can distinguish between the right- and left-handed helices. The  $\alpha$ -helices found in nature, however, are only right-handed. The model in which only right-handed helices are favored should include terms related to the chirality of the chain conformation. The chirality can be given by  $sign[(\mathbf{v}_{i-1} \times \mathbf{v}_i) \cdot \mathbf{v}_{i+1}]$ , where a negative sign means a left-handed conformation and a positive sign means a right-handed conformation (Kolinski et al., 1995).

In the following sections, the Go-like sequences without the steric constraints will be denoted by the symbols associated with the targets: H10, H16, H24, B10, B16, B15. On the other hand, the sequences constructed with the additional steric constraints will be labeled as  $\tilde{H}10$ ,  $\tilde{H}16$ ,  $\tilde{H}24$ ,  $\tilde{B}10$ ,  $\tilde{B}16$ ,  $\tilde{B}15$ .

### Dynamical equations and the thermostat

The motion of the model secondary structures of proteins can be described by the Langevin equation

$$m\ddot{\mathbf{r}} = -\gamma\dot{\mathbf{r}} + F_c + \Gamma \quad (9)$$

where  $\mathbf{r}$  is a generalized coordinate of a bead,  $m$  is the monomer's mass,  $F_c = -\nabla_r E_p$  is the conformation force,  $\gamma$  is a friction coefficient and  $\Gamma$  is the random force which is introduced to balance the energy dissipation caused by friction. Both the friction and the random force represent the effects of the solvent and they control the temperature (Grest & Kremer, 1986).  $\Gamma$  is assumed to be drawn from the Gaussian distribution with the standard variance related to temperature by

$$\langle \Gamma(0)\Gamma(t) \rangle = 2\gamma k_B T \delta(t), \quad (10)$$

where  $k_B$  is the Boltzmann constant,  $T$  is temperature,  $t$  is time and  $\delta(t)$  is the Dirac delta function.

The Langevin equations are integrated using the fifth order predictor-corrector scheme (Allen & Tildesley, 1987). The friction and random force terms are included in the form of a noise perturbing the Newtonian motion at each integration step. In the case of the model with the steric constraints, the forces associated with the angle-dependent potentials are calculated through a numerical determination of the derivatives of the potential.

In the following, the temperature will be measured in the reduced units of  $\epsilon/k_B$ . The integration time step is taken to be  $\Delta t = 0.005\tau$ , where  $\tau$  is a characteristic time unit. At low values of friction,  $\tau$  coincides with the period of oscillations,  $\tau_m$  near the Lennard-Jones minimum and is equal to  $\sqrt{ma^2/\epsilon}$ , where  $a$  is a Van der Waals radius of the amino acid residues. The value of  $a$  is chosen to be equal to  $5\text{\AA}$ , and this value is roughly equal to  $\langle \sigma_{ij} \rangle$ . As estimated by Veithshans et al. (1997), the typical values of  $m$  is  $3 \times 10^{-22}g$  and  $\epsilon$  is of the order of  $1\text{kcal/mol}$ , hence  $\tau$  is roughly equal to  $3\text{ps}$ . The period  $\tau_m$ , however, depends on the friction coefficient  $\gamma$  discussed in ref. (Veithshans et al., 1997; Klimov & Thirumalai, 1997). Most of our simulations are performed with  $\gamma = 10m\tau^{-1}$  which is 5 times higher than a standard choice in molecular dynamics studies of liquids. Higher values of  $\gamma$  may be actually more realistic. For a single aminoacid in water, an effective  $\gamma$  has been argued to be even of order  $50m/\tau$  (Veithshans et al., 1997; Klimov & Thirumalai, 1997). However, the MD code becomes unstable for too high  $\gamma$ 's. The dependence of the folding characteristics on  $\gamma$  will be discussed later in this study.

### DETERMINATION OF THE NATIVE BASIN

One problem that is encountered when studying off-lattice models is providing a definition of what small distortion away from the native state can still be considered as belonging to the native state. In other words - what is the definition of the native basin (which should not to be confused with the folding funnel)? Answering this question is important when calculating the folding time (is the system already in the native basin?) and when calculating the equilibrium stability of the basin. A need for delineation of the native basin does not arise in lattice models due to the discretization of the possible shapes - there, it is just one conformation.

The delineation of the native basin can be accomplished by considering the conformational distance,  $\delta$ , away from the native state.  $\delta$  is given by

$$\delta^2 = \frac{2}{N^2 - 3N + 2} \sum_{i=1}^{N-2} \sum_{j=i+2}^N (r_{ij} - r_{ij}^{NAT})^2, \quad (11)$$

where  $r_{ij}$  and  $r_{ij}^{NAT}$  are the monomer to monomer distances in the given structure and in the native state respectively. The distance  $\delta$  is measured in  $\text{\AA}$ .

We estimate the characteristic size of the native basin by using the shape distortion method proposed by Li and Cieplak (1999). The method is based on monitoring the conformational distance to the native state as a function of time and it considers trajectories that originate from the native state. At a sufficiently large time scale the conformational distance saturates below some critical temperature,  $T_c$ . The saturation value of the distance at this temperature,  $\delta_c$ , is used for the estimated native basin's size and the results are found to be consistent with the quench-obtained sampling of the local energy minima of the system. At the same time,  $T_c$  has been found (Li & Cieplak, 1999) to be a measure of the folding temperature  $T_f$ .  $T_f$  itself is defined as a temperature at which the equilibrium probability of finding the system in its native basin crosses  $\frac{1}{2}$ .

An illustration of the shape distortion method for sequences H16 and B16 is shown in Figure 2. For each of these sequences the dependence of  $\langle \delta^2 \rangle_t^{1/2}$  on time is shown for two temperatures: a critical  $T_c$ , when the saturation is still observed, and a somewhat higher  $T$ , when there is no saturation which is interpreted as exiting the "trap" provided by the native basin. The estimated basin size for sequences H16 and B16 are  $0.6\text{\AA}$  and  $0.15\text{\AA}$  respectively. Notice that sequence H16 has much larger basin than sequence B16 and the corresponding  $T_c$  is also much higher for H16.

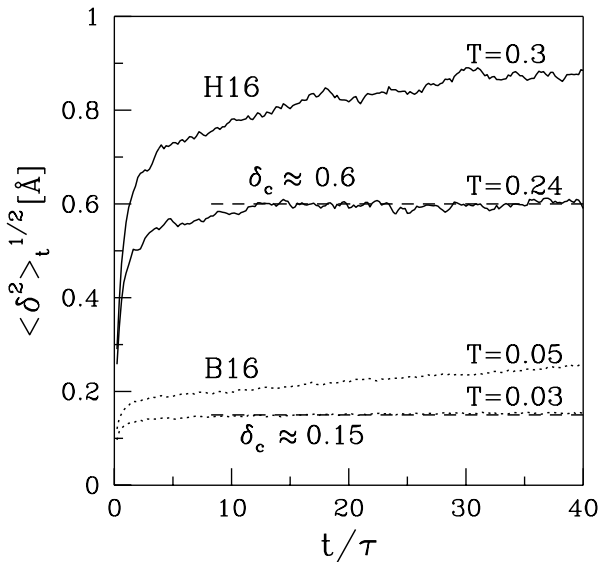


Fig. 2. The average root mean square distance to the native state as a function of time when the sequence is placed in its native conformation. The figure is for sequences H16 and B16 and for the reduced temperatures as indicated. The results are averaged over 500 trajectories which differ in the strings of the random noise.

Table I summarizes the values of  $\delta_c$  and  $T_c$  for all of the sequences studied. It also shows the number of na-

tive contacts in the native state,  $N_c$ , the conformational distance from the native state to the closest local minimum,  $\delta_1$ , and the values of  $T_f$  obtained in the next sections. The closest local minimum to the native state is found by a multiple quenching from the random conformations in a low  $T$  MD trajectory. Notice that for the  $\beta$ -structures, the models with the steric constraints yield a larger  $\delta_c$  compared to the models without the constraints. The basin sizes for the  $\alpha$ -helices, on the other hand, are comparable. In most cases, we have found that  $\delta_c$  is somewhat smaller than  $\delta_1$ . This is not so, however, in the case of  $\tilde{H}24$  and  $\tilde{B}15$ . We interpret this as a necessity to delineate the native basin by more than one isotropic parameter  $\delta_c$  and yet we shall use it here as a simple way to provide estimates.

TABLE I. The number of native contacts in the native conformations,  $N_c$ , the conformational distance from the native state to the closest local minimum,  $\delta_1$ , the native basin size,  $\delta_c$ , the critical temperature of the shape distortion,  $T_c$ , the folding temperature,  $T_f$ , and the temperature of the fastest folding,  $T_{min}$ , for the sequences studied\*.

SEQ	$N_c$	$\delta_1[\text{\AA}]$	$\delta_c[\text{\AA}]$	$T_c$	$T_f$	$T_{min}$
H10	21	0.8248	0.50(3)	0.23(1)	0.24(1)	0.25(3)
H16	39	0.6594	0.60(3)	0.24(1)	0.24(1)	0.30(3)
H24	63	0.5430	0.53(3)	0.19(1)	0.20(1)	0.30(3)
B10	18	0.2588	0.15(2)	0.035(2)	0.033(2)	0.08(1)
B16	33	0.2288	0.15(2)	0.030(2)	0.027(2)	0.07(1)
B15	33	0.1382	0.13(2)	0.030(2)	0.029(2)	0.05(1)
$\tilde{H}10$	21	0.8133	0.46(3)	0.30(1)	0.31(1)	0.50(5)
$\tilde{H}16$	39	0.6356	0.55(3)	0.30(1)	0.29(1)	0.45(3)
$\tilde{H}24$	63	0.3896	0.55(5)	0.24(2)	0.24(1)	0.36(3)
$\tilde{B}10$	18	0.3178	0.25(2)	0.20(1)	0.20(1)	0.35(5)
$\tilde{B}16$	33	0.2801	0.25(2)	0.20(1)	0.21(1)	0.35(2)
$\tilde{B}15$	33	0.2045	0.30(2)	0.22(1)	0.20(1)	0.35(2)

\* The numbers in parenthesis indicate the error bars.

## PHONONIC SPECTRA AND STABILITY

We now consider elastic vibrations of the systems around their native states and ask if the phononic spectra relate to the folding temperature.

Let  $u_{i\alpha}$  denote a small displacement of bead  $i$  in the direction  $\alpha$  ( $\alpha = x, y, z$ ) from its native position. In the harmonic approximation, the motion of the system is governed by a set of  $3N$  coupled equations (Callaway, 1974)

$$-m\omega^2 u_{i\alpha} = \sum_{j=1}^N \sum_{\beta} k_{ij}^{\alpha\beta} u_{j\beta} , \quad (12)$$

where  $\omega$  is an angular frequency, and  $k_{ij}^{\alpha\beta}$  are the second

derivatives of the potential energy taken at the native conformation:

$$k_{ij}^{\alpha\beta} = \left. \frac{\partial^2 E_p}{\partial u_{i\alpha} \partial u_{j\beta}} \right|_{\mathbf{u}=0}. \quad (13)$$

We diagonalize these equations with the use of the Jacobi transformation method (Press et al., 1993) and determine the phononic spectrum from the eigenvalues. The elastic constant matrix  $\{k_{ij}^{\alpha\beta}\}$  is real and symmetric. For the models without the steric constraints, when only the pair-wise interactions are present, the diagonal elements are equal to the negative of the sum over all of the off-diagonal elements in the same row (or column). In the case of the models with the steric constraints, however, the potentials acquire many-body components. The elastic constants  $k_{ij}^{\alpha\beta}$  are calculated by freezing all beads but one, at a time, in their native positions and by measuring the resulting increase in the force when the unfrozen bead is displaced in a given direction. This is done numerically and then a displacement of  $10^{-7}\text{\AA}$  has been found to yield a sufficient accuracy. The elastic constants, when measured along a line connecting the two beads, are of order of  $2\epsilon/\text{\AA}^2$  for both the contact and peptide bond interactions. The steric constraints enhance the elastic constants by up to a factor of 2. Naturally, this will increase the stability.

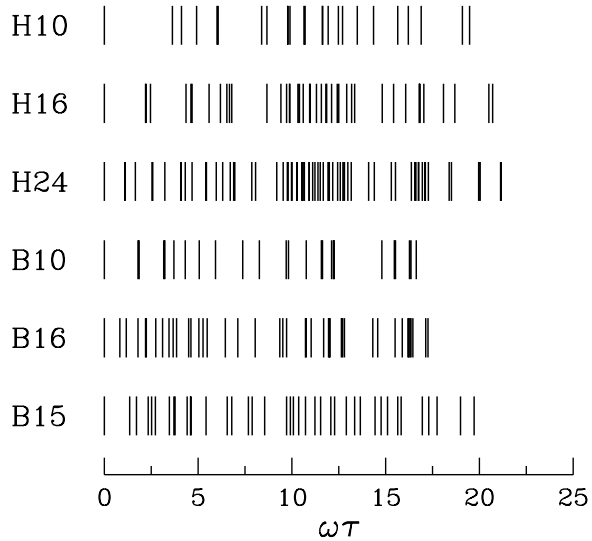


Fig. 3. The phononic spectra for the sequences modeled without the steric constraints. The values of  $\omega_1\tau$  given in rad are, top to bottom: 3.635, 2.195, 1.080, 1.789, 0.815, 1.339.

The phononic spectra for the models without and with the steric constraints are shown in Figures 3 and 4 respectively. Each spectrum contains 6 zero frequency modes which correspond to the translational and rotational degrees of freedom of the system as a whole. The first excited mode, of frequency  $\omega_1$ , defines the frequency gap in

the spectrum. We observe that the gap correlates with the thermodynamic stability: generally, the bigger the  $T_f$ , the bigger the gap. Specifically, we notice that, for a given kind of structure,  $\omega_1$  decreases as the system size increases. Furthermore, the gaps for the  $\alpha$ -helices are larger than those for the  $\beta$ -structures for a given chain length. Finally, adding the steric constraints shifts the whole spectra towards higher frequencies.

An energy associated with a mode depends on its amplitude. If an amplitude of vibrations of a single bead is of order  $u_0$ , then the energy of the first excited mode,  $E_1$ , is of order  $Nm\omega_1^2 u_0^2$ . As an estimate of  $u_0$ , we may take  $\approx 0.1a$  which is an analog of the Lindemann criterion for melting of the solids. Note that  $\omega_1$  is expressed in units of  $1/\tau$ , where  $\tau = \sqrt{ma^2/\epsilon}$  and  $a = 5\text{\AA}$ . Thus our estimates for  $E_1/\epsilon$  are 1.32, 0.77 and 0.28 for H10, H16 and H24 respectively. This indicates a decrease of stability with  $N$  but the correlation with the actual value of  $T_f$  is weak.

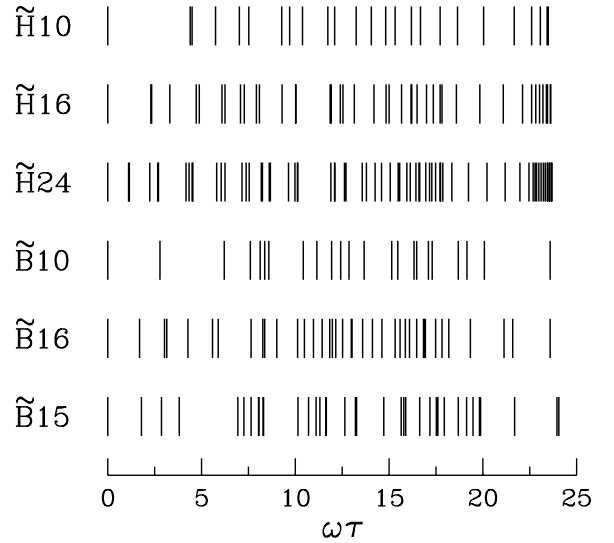


Fig. 4. Same as Fig. 3 but for the sequences modeled with the steric constraints. The values of  $\omega_1\tau$  are, top to bottom: 4.385, 2.290, 1.105, 2.775, 1.695, 1.795.

## FOLDING PROPERTIES IN MODELS WITHOUT THE STERIC CONSTRAINTS

### Equilibrium properties

Before we discuss the folding process, we first provide a thermodynamic characterization of the sequences studied. We focus on three parameters:  $\mathcal{P}_0$ ,  $C$ , and  $\chi$ . These denote the probability of being in the native basin, the specific heat per bead, and the structural susceptibility respectively. The thermodynamic stability may be characterized by  $T_f$  at which  $\mathcal{P}_0$  crosses  $\frac{1}{2}$ . The specific heat is defined by the energy fluctuations:

$$C = \frac{1}{N} \frac{\langle E^2 \rangle - \langle E \rangle^2}{T^2}, \quad (14)$$

where  $E$  is the total energy (kinetic and potential) of the system. The brackets denote the thermodynamic average. The structural susceptibility is defined in terms of the structural overlap function (Veithshans et al., 1997) which is given by

$$\chi_s = 1 - \frac{2}{N^2 - 3N + 2} \sum_{i=1}^{N-2} \sum_{j=i+2}^N \Theta(\delta_c - |r_{ij} - r_{ij}^{NAT}|), \quad (15)$$

where  $\Theta(x)$  is the Heavyside function.  $\chi$  is then a measure of fluctuations in  $\chi_s$ :

$$\chi = \langle \chi_s^2(T) \rangle - \langle \chi_s(T) \rangle^2 \quad (16)$$

The maximum in  $C$ , when plotted against  $T$ , corresponds to the collapse transition temperature  $T_\theta$  at which there is a transition from random coil to compact conformation. The maximum in  $\chi$  may be interpreted as a signature of the folding temperature  $T_f$  (Camacho & Thirumalai, 1993; Thirumalai, 1995). It has been suggested (Klimov & Thirumalai, 1996) that a small difference between these two temperatures is indicative of good folding properties. As a practical criterion for good foldability one may take the parameter  $\sigma_T = (T_\theta - T_f)/T_\theta$  to be less than 0.4 (Veithshans et al., 1997).

We calculate the thermodynamic parameters by averaging over many long MD trajectories using the native state as the starting configuration to make sure that the evolution take space in the right parts of the phase space. For each temperature, the times used for averaging in each trajectory are between 500 and 2000 $\tau$  depending on the chain length. The first 1000 $\tau$  are not taken into account when averaging. We used as many trajectories as needed to provide stable characterization. In practice, considering of order 50 trajectories have been found to be sufficient.

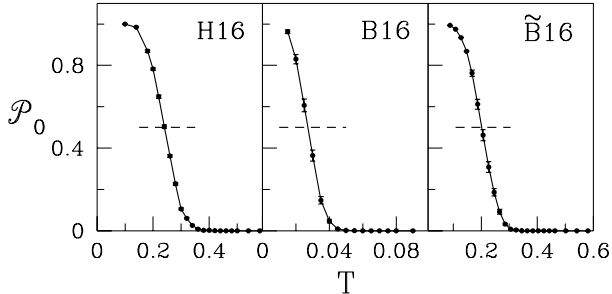


Fig. 5. The probability of being in the native basin as function of temperature for the sequences with  $N=16$ . H16 and B16 are without the steric constraints. Adding the steric constraints improves the stability as seen in the case of  $\tilde{B}16$  on the right hand side.

The values of  $T_f$  are listed in Table I. They almost coincide with the values  $T_c$  obtained by the shape distortion method. One can clearly see that the stability of the helices is substantially larger than that of the  $\beta$  structures. The poor stability of the  $\beta$ -systems is a result of their flat non-compact native conformation. There are many competing local energy minima with very similar structures in the immediate neighborhood of the native state. We have checked that an increase in the off-plane zigzag like departures can bring about a significant boost to the stability. However, one of the goals of this paper is to deal with realistic geometries. We shall see, in the next section, that the extra stability that is needed will be provided by the additional steric constraints. This is also illustrated in Figure 5 for three selected sequences.

Figure 6 summarizes the thermodynamic properties of the sequences modeled without the steric constraints. The peaks of  $C$  and  $\chi$  are observed for all of the helices and  $\beta$ -systems. Notice, however, that in the case of the  $\beta$ -structures the peaks are much less pronounced. Notice also that the values of  $T_f$ , as indicated by the arrows and obtained based on monitoring  $P_0(T)$ , generally agree quite closely with the positions of the maxima in  $\chi$ . This consistency testifies about a reasonable and consistent determination of the size of the native basin. For all of the sequences studied here the parameters  $\sigma_T$  are smaller than 0.4 and thus are expected to be good folders whereas H24 shows the borderline behavior.

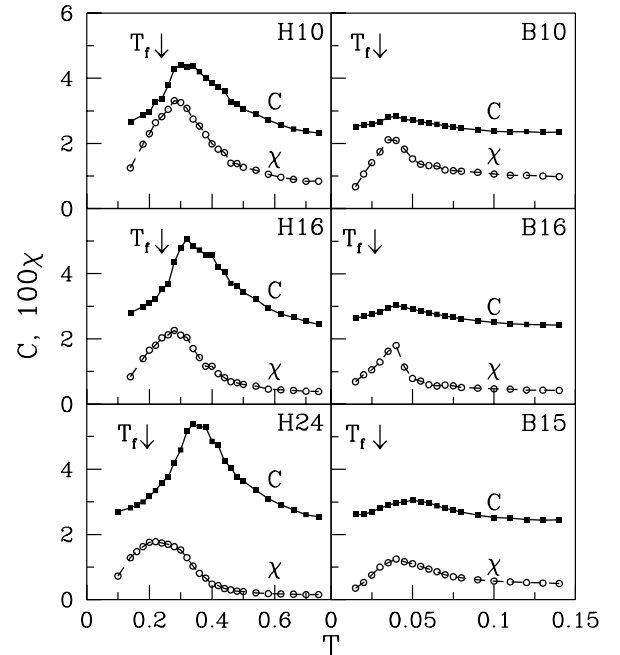


Fig. 6. The specific heat,  $C$ , and the structural susceptibility,  $\chi$ , as functions of the reduced temperature for the sequences indicated. The arrows show the values of the folding temperature as obtained through monitoring of the equilibrium probability to reside in the native basin.

## Kinetic properties

We now consider the kinetic properties of the sequences without the steric constrains. From a kinetic point of view, a sequence is considered to be a good folder if its folding temperature  $T_f$  is comparable or preferably larger than  $T_{min}$  – the temperature of the fastest folding. If this happens then there must exist a temperature range below  $T_f$  at which the native state is still easily accessible kinetically. Thus the first task in this context is to determine  $T_{min}$ .

We have studied the dynamics of the sequences by extensive MD simulations. Figure 7 shows the median folding time as a function of temperature. At each temperature the median folding time is computed based on either 100 or 200 trajectories starting from random initial conformations. The initial conformations are generated from random sets of the bond angles and dihedral angles, where the bond angles are additionally restricted to have random value between  $0^\circ$  and  $90^\circ$  so that these conformations are not compact. On the other hand, the cases with the distance between two non-bonded beads of less than  $0.8d_0$  have been also excluded in order not to violate the self-avoidance condition. Conformations generated by this method typically look like extended random coils. Figure 7 shows the expected U-shape dependence (Socci & Onuchic, 1994; see also Cieplak & Banavar, 1997) of the folding time on temperature. Notice that the  $\beta$ -sequences fold the best at a much lower range of temperatures than what is observed for the  $\alpha$ -helices. The temperature of the fastest folding  $T_{min}$  for the  $\beta$ -sequences is between 0.05 and 0.08 while for the  $\alpha$ -helices it is about 0.25 or 0.3.

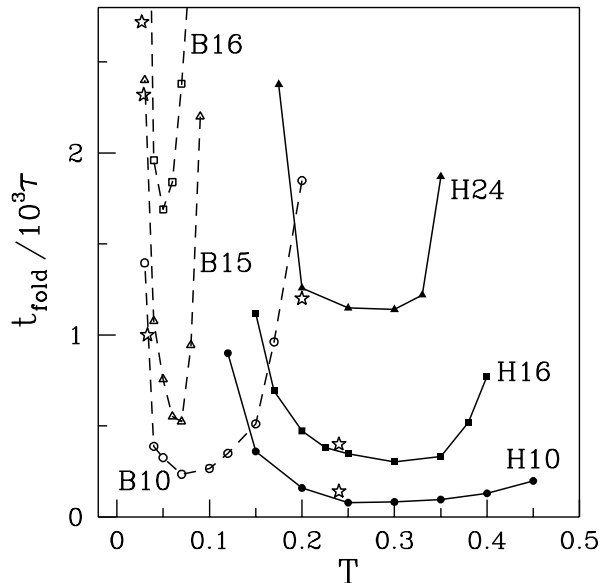


Fig. 7. The median folding time versus temperature for the sequences modeled without the steric constraints. The asterisks indicate the corresponding values of  $T_f$ .

Since for all the sequences  $T_f$  is less than  $T_{min}$ , the sequences can be considered to be either good or bad folders depending on how significantly do the folding conditions deteriorate on moving away from  $T_{min}$  to  $T_f$ . Thus it is of interest to compare the folding time at  $T_{min}$ ,  $t_1$ , to the folding time at  $T_f$ ,  $t_2$ . The  $\alpha$ -helices are good folders because for them  $t_2/t_1 < 2$ . i.e., the two times are almost the same. For the the  $\beta$ -sequences, on the other hand, these ratios are higher reflecting a much narrower temperature range in which the good folding conditions are available. For B10 and B15, for instance, the ratios  $t_2/t_1$  are about 7 and 5 respectively. Thus the  $\beta$ -sequences without the steric constraints are bad folders. Note that our kinetically derived results on the quality of folding do not fully agree with those obtained by studying the thermodynamically derived parameter  $\sigma_T$ . The reason why the thermodynamic criterion appears to be faulty may have to do with the fact that the  $\beta$ -structures studied here have a low degree of compactness. Note also the poor pronunciation of the peaks in the specific heat for the  $\beta$ -structures.

Figure 7 shows that the  $\beta$ -sequences fold more slowly than the  $\alpha$ -helices of the same chain length. For instance, the minimum folding time for  $\beta$ -hairpin B16 is about 5 times larger than for the  $\alpha$ -helix H16. Notice also that the  $\beta$ -sheet B15 folds considerably faster than the hairpin B16, though their lengths are comparable. All of these observations are consistent with the large role of the local contacts (as measured along the chain) in establishing good foldability (Unger & Moult, 1996).

Figure 7 indicates that the folding time strongly depends on the chain length. Studies of lattice models, first by Gutin et al. (1996) and recently by Cieplak et al. (1999), have pointed out that the folding time grows as a power law with the system size  $t \sim N^\lambda$ . Our calculations (Cieplak et al., 1999) have shown that for the Go sequences  $\lambda$  is about 6 for two dimensional lattice sequences and about 3 for three dimensional sequences. Here, we have checked that the folding times at  $T_{min}$  of the three sequences H10, H16, H24 are consistent by the power law with  $\lambda = 3.0 \pm 0.1$ . The agreement with the exponent obtained for the maximally compact Go lattice models is probably coincidental. One of the important conclusions suggested by Cieplak et al. (1999) is that there may exist a limit to functionality of proteins that can be demonstrated through studies of scaling of  $T_f$  and  $T_{min}$ . In the Go lattice models, as  $N$  grows,  $T_{min}$  grows indefinitely whereas  $T_f$  saturates with  $N$ . This, together with the increase in the folding times, indicates a deterioration of the folding properties with  $N$ . The data obtained for the few sizes of helices studied here (see Table I) are only partially consistent with this scenario for the behaviors of the characteristic temperatures. Note, however, that the longer a helix, or a  $\beta$ -structure, is the less compact is its native conformation and this in itself may yield a different behavior of  $T_f$  and  $T_{min}$ .

## FOLDING PROPERTIES IN MODELS WITH THE STERIC CONSTRAINTS

### Equilibrium properties

We now repeat our methodology in reference to the sequences which are modeled with the implementation of the steric constraints. The thermodynamic properties for the systems of this type are summarized in Figure 8. The values of the folding temperatures  $T_f$  are also listed in Table I. Notice that the models with the steric constraints are generally characterized by larger values of  $T_f$  than the models without such constraints. The changes are especially substantial for the  $\beta$ -structures since the resulting values of  $T_f$  become now comparable to those of the helices.

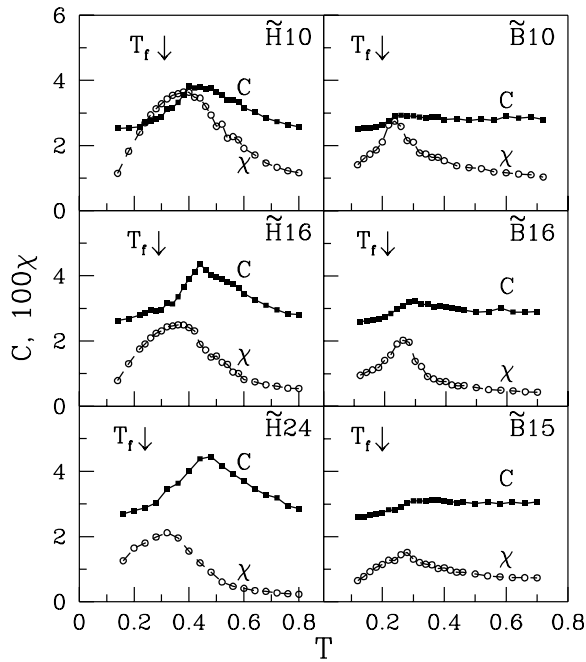


Fig. 8. Same as Figure 6 but for the sequences modeled with the steric constraints. Notice the shift in the temperature scale.

### Kinetic properties

Figure 9 shows the dependence of the folding time on temperature. The points shown are based on either 100 or 200 trajectories starting from random initial conformations. For all of the structures studied here,  $T_{min}$  also becomes larger than that in the models without the steric constraints. The time scales of folding, however, are affected to a relatively much smaller extent. For the  $\beta$ -sequences, the folding time at  $T_{min}$  practically does not change. For the  $\alpha$ -helices, on the other hand, some slowing down is observed. When comparing the  $\alpha$ -helices to the  $\beta$ -structures one concludes that the helices continue

to be faster folders but, for instance,  $\tilde{H}16$  now folds only about two times faster than  $\tilde{B}16$  at  $T_{min}$ , as opposed to the factor of five observed without the constraints.

Like in the model without steric constraints, for all the cases we still have  $T_f < T_{min}$ . Comparing the folding times at  $T_f$  and at  $T_{min}$  yields that the helices continue to be good folders ( $t_2/t_1 < 2$ ). The  $\beta$ -sequences are still bad folders but now the ratios  $t_2/t_1$  are somewhat smaller than that in the model without steric constraints. For instance, for  $\tilde{B}10$ ,  $t_2/t_1$  is about 3.

We conclude that adding the steric constraints to the Go-like interactions between the aminoacids improves the stability of the sequences, while it does not change much in the folding characteristics. The folding characteristics seem to be embedded in the very geometry of the native structure.

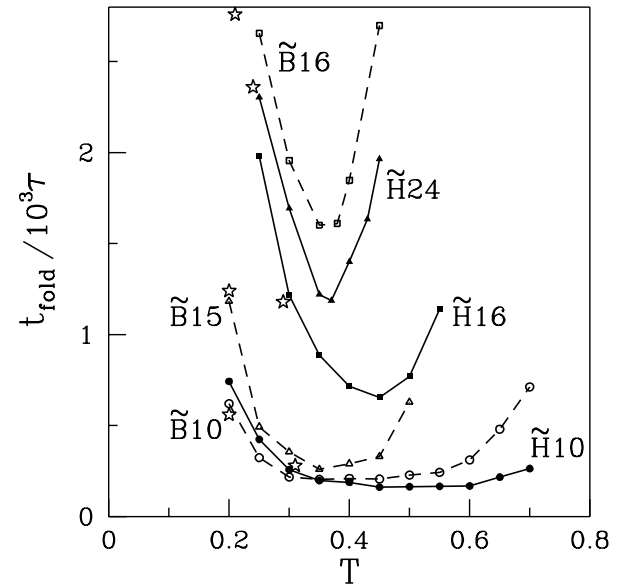


Fig. 9. Same as Figure 7 but for the sequences modeled with the steric constraints.

## THE MECHANISM OF FOLDING OF SECONDARY STRUCTURES

### Sequencing of events

In this section, we focus on identifying stages in the folding process of the model secondary structures. Specifically, we discuss orders and time scales in which specific contacts are established. We narrow our discussion now to the three following structures: the  $\alpha$ -helix  $H16$ , the  $\beta$ -hairpin  $B16$ , and the  $\beta$ -sheet  $B15$ .

By starting from random unfolded conformations we compute an average time, at which a given contact is established for the first time. Two monomers,  $i$ -th and  $j$ -th, are assumed to be in a contact if their distance is smaller than  $1.5\sigma_{ij}$ . The contact range definition of  $7.5\text{\AA}$ ,

used in the potential design procedure, is not appropriate to be used here, since each contact has a potential with its own variable  $\sigma_{ij}$ . Since the number of all native contacts is quite large we select several contacts, as indicated in Figure 10, for monitoring. The choice of the contacts is motivated by their dominant role in stabilization provided by the hydrogen bonds. The labels indicate order in which these selected contacts first appear on average. For the  $\alpha$ -helix, the folding is seen to start, statistically, at the ends (we have symmetrized the data with respect to the two ends). On the other hand both  $\beta$ -structures first fold near the turns, i.e. where the local contacts are present. Note that the contacts indicated in the helix all have the same locality index at yet the end contacts are found to be privileged. Adding the steric constraints does not change the average sequencing of the kinetic events.

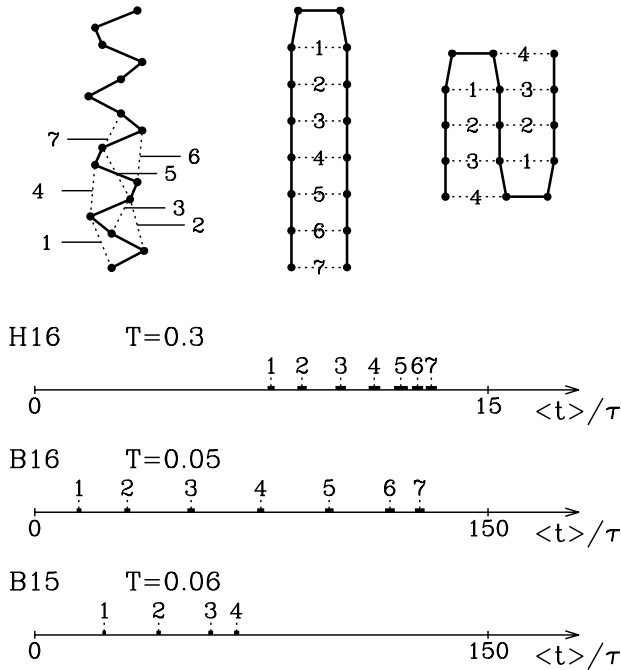


Fig. 10. Top: the contacts considered in the sequencing studies together with the number which indicates the order of the appearance. The structures are, from the left to the right, H16, B16 and H15. Bottom: the corresponding average time for a contact to appear for the first time during folding. The folding takes place at  $T_{min}$ . The results for H16 are averaged over 1000 trajectories that start from random conformations. For B16 and B15, 500 trajectories are considered. The error bars are indicated by the thicker horizontal marks.

Figures 10 and 11 show the average times to establish the contacts at  $T_{min}$  for the unconstrained and constrained Go-like models respectively. When comparing the times obtained for the  $\alpha$ -helix to the  $\beta$ -structures, note the change in the time scale. The full folding takes place in about from 10 to 20 times longer than the last of the monitored contacts is established. The general

pattern observed here is that of steps which are initially more or less evenly spaced followed by a rapid acceleration towards the end.

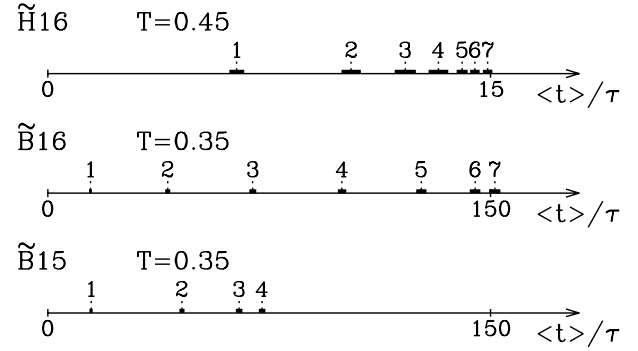


Fig. 11. Same as the bottom of Figure 10 but for the sterically constrained sequences.

Figure 12 shows the average times to establish the contacts at temperatures which are away from  $T_{min}$  – above or below. We focus on  $\tilde{H}16$  and  $\tilde{B}16$ . The results show that for sequence  $\tilde{B}16$  the sequencing of contacts does not change with temperature. For  $\tilde{H}16$ , on the other hand, the sequencing starts the same as at  $T_{min}$ , i.e. at the end points, but the canonical order becomes disrupted at the later stages. For instance, establishing contact 5 before 7 is as likely as establishing 7 before 5. Notice that, above  $T_{min}$ , establishing the basic contacts in the two structures takes about as long as at  $T_{min}$  even though the folding times got longer. On the other hand, below  $T_{min}$ , this process becomes more extended in time.

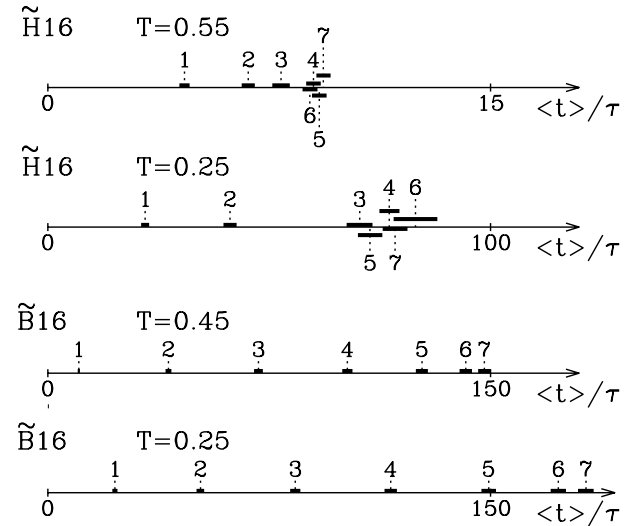


Fig. 12. The contact sequencing for sequences  $\tilde{H}16$  and  $\tilde{B}16$  at temperatures that are above or below  $T_{min}$ .

### Examples of the trajectories

Notice that the first appearance of the last contact that is monitored does not coincide yet with the full folding because a substantial time is still needed to lock precisely into the native basin. In fact, getting to the stage where the last contact starts giving contribution to the energy takes of order of only from 5% to 10% of the full folding time. This time roughly corresponds to the collapse of the chain.

This is illustrated in Figures 13 and 14, for  $\tilde{H}16$  and  $\tilde{B}16$  respectively, where examples of single trajectories at  $T_{min}$  are shown. The trajectories are characterized by their total energy,  $E$ , potential energy,  $E_p$ , the radius of gyration,  $R_g$ , conformational distance away from the native state and the number of all native contacts,  $N_c$ , (not only of those few that were discussed in the context of sequencing) present. All of these parameters depend on time essentially monotonically. The establishment of the short contacts takes place rapidly and then the system spends most of the folding time “floating” near the native basin until it really finds it. Thus what takes most of the time in folding is the process of search. This process is thus governed more by kinetics than by energetics.

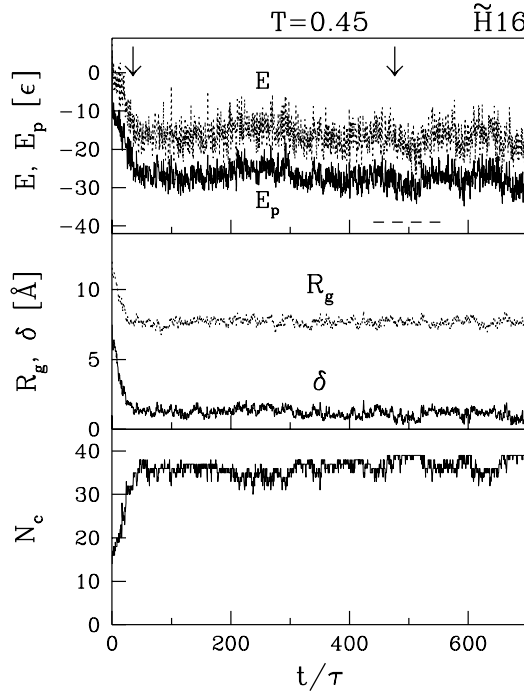


Fig. 13. A typical folding trajectory at  $T_{min}$  for sequence  $\tilde{H}16$ . In the top panel the left arrow indicates when the last contact appears for the first time, and the right arrow indicates when folding takes place, i.e.  $\delta < \delta_c$ . The horizontal dash line indicates the energy of the native state.

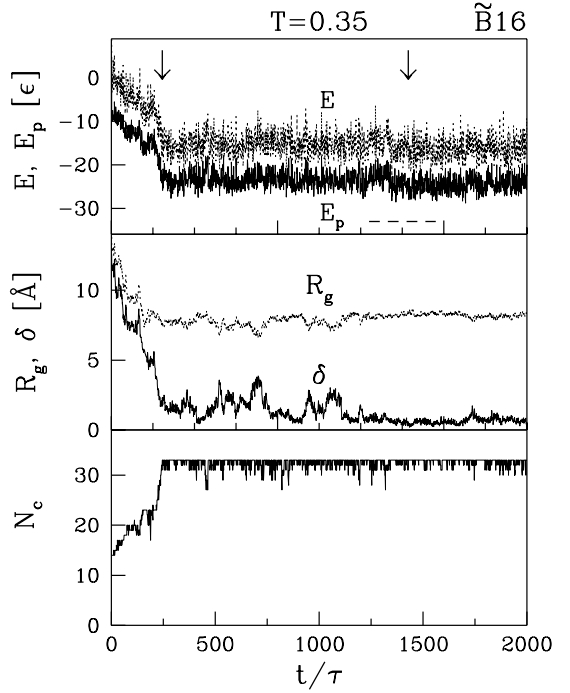


Fig. 14. Same as Figure 12 but for sequence  $\tilde{B}16$ .

### Dependence on the viscous friction

We now examine how do the folding properties depend on the viscosity. So far, the results of all of the simulations shown here were obtained with  $\gamma = 10m/\tau$ . We have checked that for sequence  $H16$ ,  $T_{min}$  does not depend on the friction and is equal to 0.3 if  $\gamma > 0.2m/\tau$ . At very low friction, i.e. when  $\gamma < 0.2m/\tau$ , we observe some decrease of  $T_{min}$ . For instance,  $T_{min}$  is about 0.05 for  $\gamma = 0.005m/\tau$ . Since  $T_f$  cannot depend on  $\gamma$ , at this very low value of friction the sequence becomes an excellent folder. However, such small values of  $\gamma$  are very unrealistic for proteins (Klimov & Thirumalai, 1997). We have also checked that other thermodynamic properties do not depend on  $\gamma$ . Figure 15 shows the dependence of the median folding time on friction for a wide range of  $\gamma$ , at  $T = 0.3$  and also at  $T_{min}$  for  $\gamma < 0.2m/\tau$ . Notice that there is a minimum of the folding time at some intermediate friction. The folding time grows not only at higher friction, as  $\gamma$  increases, but also at very low friction, as  $\gamma$  decreases towards 0. There is no folding at  $\gamma = 0$ , when the total energy of the system is conserved – a coupling to a heat reservoir is essential for folding. The optimal value of  $\gamma$ , at which folding is the fastest, is in a range of from 0.2 to 0.5. This observation is in agreement with the results of Klimov and Thirumalai on the viscosity dependence of the folding rate (Klimov & Thirumalai, 1997). Notice that Klimov and Thirumalai have determined foldability rates and not the folding times themselves. We also observe that for  $\gamma$  between 1 and 30, the folding time of sequence  $H16$  grows almost linearly

with  $\gamma$ , as shown in the inset of Figure 15. By extrapolation we estimate that for  $\gamma = 50m/\tau$  the folding time for H16 would be  $1500\tau$  (for  $\tilde{H}16$  it would be about  $3000\tau$ ). Veitshans et al. (1997) have estimated that at this apparently more realistic value of friction, corresponding to the case of a single aminoacid in a water solution at room temperature, the time unit of  $\tau$  should be about  $3\text{ns}$ . Hence our estimate of the folding time of a 16-monomer  $\alpha$ -helix is from 4 to  $10\ \mu\text{s}$ . If we assume that for the  $\beta$ -structures the folding time also scales linearly with  $\gamma$ , then the time scale for the formation of a 16-monomer  $\beta$ -hairpin would range from 24 to  $30\ \mu\text{s}$ . For comparison, experimental results have shown that a  $\beta$ -hairpin consisting of 16 aminoacids can fold as fast as  $6\ \mu\text{s}$  at room temperature (Munoz et al., 1997). An  $\alpha$ -helix of the same length folds 30 times faster. Notice that our estimates yield larger folding times than observed in experiments but the orders of magnitude agree.

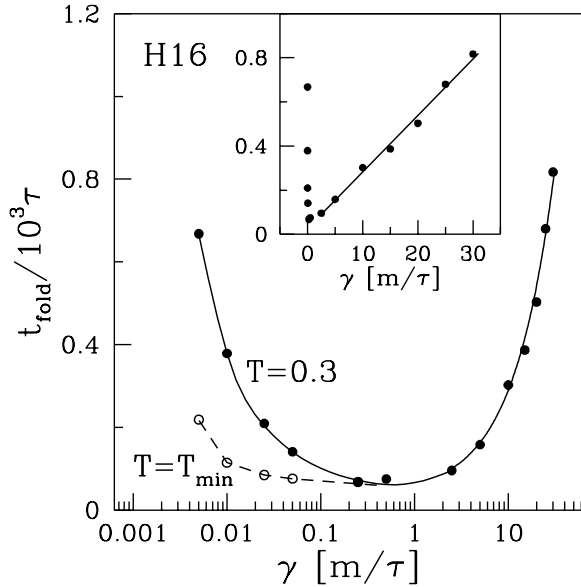


Fig. 15. The median folding time at  $T = 0.3$  (continuous line) as function of the friction coefficient,  $\gamma$ , for sequence H16. For  $\gamma < 0.2m/\tau$ ,  $T_{min}$  becomes smaller than 0.3 and the folding times at  $T = T_{min}$  are shown for several values of  $\gamma$  (discontinuous line). For  $\gamma > 0.2m/\tau$ ,  $T_{min}$  is equal to 0.3. The points are based on 200 trajectories. The inset shows the dependence at  $T = 0.3$  in a non-logarithmic scale of  $\gamma$ , where for the higher values of  $\gamma$ , the points are fitted by a straight line.

#### Folding with one end fixed

Finally, we examine a special case, when one end of the chain is fixed during folding. This is relevant to the process of protein synthesis: one end can be thought of as being momentarily glued to the surface of a ribosome until the whole protein is constructed by adding new segments (Stryer, 1993). In the synthesis process, the pro-

tein folds as it is being produced and its length extends. At each instant, however, one end of the protein can be considered pinned.

Figure 16 shows that the helix H16 with the end bead fixed has a considerably lower value of  $T_{min}$ , compared to no clamping, and it generally folds faster at low temperatures. pinned folds faster below  $T_{min}$  and is characterized by a significantly lowered  $T_{min}$ . We have also found that  $T_f$  is not affected by the pinning. Thus the helix becomes a much better folder. On the other hand, as seen in Figure 16, the contact sequencing becomes somewhat disturbed. Folding starts at the unclamped end. After the initial stage, many contacts get established almost simultaneously in an avalanche-like process. Then there is a large gap in time before the last contact, near the clamped end, comes into place.

Analyzing the phononic spectrum of the pinned helix H16 yields  $\omega_1\tau \approx 1.964$  for the first excited mode which is almost the same as for H16 without the pinning.

For the  $\beta$ -sequences the different scenario is different: the pinned  $\beta$ -structures seem to fold slower than the unpinned ones. For instance, fixing one end of sequence B16 increase the folding time by about 60%, at  $T = 0.05$ . The pinned B10 also folds slower, but not significantly slower.

Our results indicate that the process of protein synthesis itself may accelerate the folding process when a helix part is being produced. Short  $\beta$ -structures may introduce some slowing down.

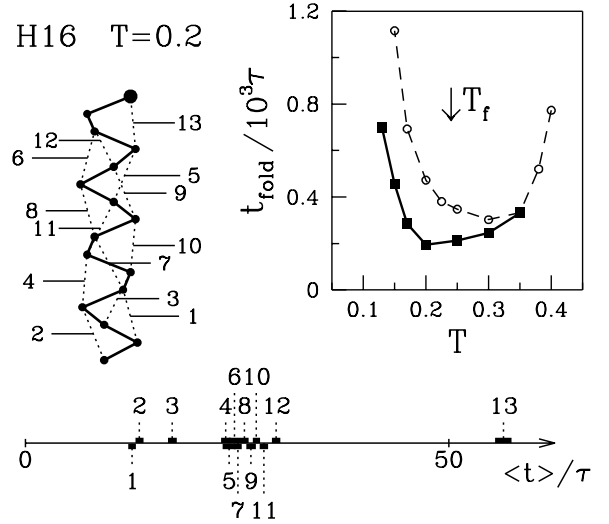


Fig. 16. The order of contact appearance together with the average times for the contacts to be established for the first time for sequence H16 with one end monomer fixed. The fixed monomer is shown enlarged. The results are averaged over 1000 trajectories at  $T_{min}$ . The inset compares the temperature dependencies of the median folding time for the situation in which the end monomer is (solid line) or is not (broken line) clamped.

## CONCLUSIONS

In summary, we have studied the Go-like models of off-lattice secondary structures of proteins. We have provided a systematic characterization of both equilibrium and kinetic properties of these models. Models with the steric constraints were endowed with better thermodynamic stability. The stability can be assessed from the phononic spectra. The folding times strongly depend on the system size and on the geometry of the native state. The  $\alpha$ -helices, which are stabilized merely by the local contacts appear to have much better folding properties than the  $\beta$ -structures. However, it should be noted that for both kinds of the structures none of the models is a very good folder –  $T_f$  is always smaller than  $T_{min}$ , – although the choice of the native basin size  $\delta_c$  has been made consistently by the shape distortion technique. We have checked that if one uses a somewhat larger  $\delta_c$  then this results in an increase in the effective values of both  $T_f$  and  $T_{min}$  and thus their ordering remains unchanged. The kinetic criterion for good foldability does not appear to be compatible with the thermodynamic criterion provided by Klimov & Thirumalai (1996) in the case of the  $\beta$ -sequences. We speculate that this may be related to the low compactness level of their native structures. Folding of the secondary structures at  $T_{min}$  proceeds, on average, through a well defined sequence of events. That sequencing may become more complicated in proteins when several secondary structures compete when folding. We intend to explore this issue later.

## ACKNOWLEDGMENTS

The idea of this project arose in discussions with Jayanth R. Banavar, whose subsequent interest and encouragement were vital for its completion. Many discussions with M. S. Li are also appreciated. We also thank M. Geller for pointing out to us that the folding process may be affected by the pinning. This work was supported by KBN (Grant No. 2P03B-025-13).

## REFERENCES

Allen MP, Tildesley DJ. 1987. Computer simulation of liquids. New York: Oxford University Press.

Becker OM, Karplus M. 1997. The topology of multidimensional potential energy surfaces: Theory and application to peptide structure and kinetics. *J Chem Phys* 106:1495-1517.

Blanco F, Ramirez-Alvarado M, Serrano L. 1998. Formation and stability of  $\beta$ -hairpin structures in polypeptides. *Curr Opin in Struct Biol* 8:107-111.

Boczko EM, Brooks CL. 1995. III. First-principles calculation of the folding free energy of a three-helix bundle protein. *Science* 269:393-396.

Callaway J. 1974. Quantum Theory of the Solid State. New York and London: Academic Press.

Camacho CJ, Thirumalai D. 1993. Kinetics and thermodynamics of folding in model proteins. *Proc Natl Acad Sci USA* 90:6369-6372.

Chan HS, Dill KA. 1993. The protein folding problem. *Phys Today* 46(2):24-32.

Chan HS, Dill KA. 1994. Transition states and folding dynamics of proteins and heteropolymers. *J Chem Phys* 100:9238-9257.

Chan HS, Dill KA. 1998. Protein folding in the landscape perspective: chevron plots and non-Arrhenius kinetics. *Proteins* 30(1):2-33.

Cieplak M, Banavar JR. 1997. Cell dynamics of folding in two dimensional model proteins. *Folding Des* 2:235-245.

Cieplak M, Henkel M, Karbowski J, Banavar JR. 1998. Master equation approach to protein folding and kinetic traps. *Phys Rev Lett* 80:3654-3657.

Cieplak M, Hoang TX, Li MS. 1999. Scaling of folding properties in simple models of proteins. *Phys Rev Lett* 83:1684-1687.

Clementi C, Maritan A, Banavar JR. 1998. Folding, design and determination of interaction potentials using off-lattice dynamics of model heteropolymers. *Phys Rev Lett* 81:3287-3290.

Dill KA, Bromberg S, Yue S, Fiebig K, Yee KM, Thomas DP, Chan HS. 1995. Principles of protein folding – A perspective from simple exact models. *Protein Sci* 4:561-602.

Dokholyan NV, Buldyrev SV, Stanley HE, Shakhnovich EI. 1998. Discrete molecular dynamics studies of the folding of a protein-like model. *Folding Des* 3:577-587.

Dokholyan NV, Buldyrev SV, Stanley HE, Shakhnovich EI. 1998. Identifying the protein folding nucleus using molecular dynamics. *cond-mat* 9812284.

Duan Y, Kollman PA. 1998. Pathways to a protein folding intermediate observed in a 1-microsecond simulation in aqueous solution. *Science* 282:740-744.

Garstecki P, Hoang TX, Cieplak M. 1999. Energy landscapes, supergraphs, and “folding funnel” in spin systems. *Phys Rev E* 60:3219-3226.

Go N, Abe H. 1981. Noninteracting local-structure model of folding and unfolding transition in globular proteins. I. Formulation. *Biopolymers* 20:991-1011.

Grest GS, Kremer K. 1986. Molecular dynamics simulation for polymers in the presence of a heat bath. *Phys Rev A* 33:3628-31.

Gutin AM, Abkevich VI, Shakhnovich EI. 1996. Chain length scaling of protein folding time. *Phys Rev Lett* 77:5433-5436.

Hardin C, Luthey-Schulten Z, Wolynes PG. 1999. Backbone Dynamics, fast folding, and secondary structure formation in helical proteins and peptides. *Proteins Struct Funct Genet* 34:281-294.

He S, Scheraga HA. 1998. Brownian dynamics simulations of protein folding. *J Chem Phys* 108:287-300.

Iori G, Marinari E, Parisi G. 1991. Random self-interacting chains: a mechanism for protein folding. *J Phys A* 24:5349-5362.

Irback A, Peterson C, Potthast F, Sommelius O. 1997. Local interactions and protein folding: a three-dimensional off-lattice approach. *J Chem Phys* 107:273-282.

Irback A, Peterson C, Potthast F. 1997. Identification of amino acid sequences with good folding properties in an off-lattice model. *Phys Rev E* 55:860-867.

Karplus M. 1987. Molecular dynamics simulations of proteins. *Physics Today* October:68-72.

Klimov DK, Thirumalai D. 1996. A criterion that determines the foldability of proteins. *Phys Rev Lett* 76:4070-4073.

Klimov DK, Thirumalai D. 1997. Viscosity dependence of the folding rates of proteins. *Phys Rev Lett* 79:317-320.

Kolinski A, Godzik A, Skolnick J. 1995. A reduced model of short range interactions in polypeptide chains. *J Chem Phys* 103:4312-4322.

Li A, Daggett V. 1994. Characterization of the transition state of protein unfolding by use of molecular dynamics: chymotrypsin inhibitor 2. *Proc Natl Acad Sci USA* 91:10430-10434.

Li H, Helling R, Tang C, Wingren N. 1996. Emergence of preferred structures in a simple model of protein folding. *Science* 273:666-669.

Li MS, Cieplak M. 1999. Delineation of the native basin in continuum models of proteins. *J Phys A* 32:5577-5584.

Li MS, Cieplak M. 1999. Folding in two-dimensional off-lattice models of proteins. *Phys Rev E* 59:970-976.

Micheletti C, Banavar JR, Maritan A, Seno F. 1999. Protein structures and optimal folding from a geometrical variational principle. *Phys Rev Lett* 82:3372-3375.

Miller MA, Wales DJ. 1999. Energy Landscape of a Model Protein. *J Chem Phys* 111:6610-6616.

Miyazawa S, Jernigan RL. 1985. Estimation of effective interresidue contact energy from protein crystal structures: quasi-chemical approximation. *Macromolecules* 18:534-552.

Munoz V, Thompson PA, Hofrichter J, Eaton WA. 1997. Folding dynamics and mechanism of  $\beta$ -hairpin formation. *Nature* 390:196-199.

Press WH, Flannery BP, Teukolsky SA, Vetterling WT. 1993. Numerical Recipes in FORTRAN. Cambridge, UK: Cambridge University Press.

Sali A, Shakhnovich E, Karplus M. 1994. How does a protein fold? *Nature* 369:248-251.

Socci ND, Onuchic JN. 1994. Folding kinetics of proteinlike heteropolymers. *J Chem Phys* 101:1519-1528.

Stryer L. 1995. Biochemistry. New York: WH Freeman and Company.

Thirumalai D. 1995. From minimal models to real proteins: Time scales for protein folding kinetics. *J Phys (Paris)* I 5:1457-1467.

Unger R, Moult J. 1996. Local interactions dominate folding in a simple protein model. *J Mol Biol* 259:988-994.

Veitshans T, Klimov D, Thirumalai D. 1997. Protein folding kinetics: time scales, pathways and energy landscapes in terms of sequence-dependent properties. *Folding Des* 2:1-22.

Vendruscolo M, Maritan A, Banavar JR. 1997. Stability threshold as a selection principle for protein design. *Phys Rev Lett* 78:3967-3970.

Wolynes PG. 1996. Symmetry and the energy landscapes of biomolecules. *Proc Natl Acad Sci USA* 93:14249-14255.

Zhou Y, Hall CK, Karplus M. 1996. First-order disorder-to-order transition in an isolated homopolymer model. *Phys Rev Lett* 77:2822-2825.

Zhou Y, Karplus M. 1999. Interpreting the folding kinetics of helical proteins. *Nature* 401:400-403.